

JAERI - M  
87-130

COMPUTATION OF TOKAMAK EQUILIBRIA  
WITH STEADY FLOW

August 1987

Wolfgang KERNER\* and Shinji TOKUDA

JAERI-Mレポートは、日本原子力研究所が不定期に公刊している研究報告書です。  
入手の問合わせは、日本原子力研究所技術情報部情報資料課（〒319-11茨城県那珂郡東海村）あて、お申しこしてください。なお、このほかに財団法人原子力弘済会資料センター（〒319-11 茨城県那珂郡東海村日本原子力研究所内）で複写による実費頒布をおこなっております。

JAERI-M reports are issued irregularly.

Inquiries about availability of the reports should be addressed to Information Division  
Department of Technical Information, Japan Atomic Energy Research Institute, Tokai-  
mura, Naka-gun, Ibaraki-ken 319-11, Japan.

©Japan Atomic Energy Research Institute, 1987

編集兼発行 日本原子力研究所  
印刷 (株)高野高速印刷

Computation of Tokamak Equilibria With Steady Flow

Wolfgang KERNER\* and Shinji TOKUDA

Department of Thermonuclear Fusion Research

Naka Fusion Research Establishment

Japan Atomic Energy Research Institute

Naka-machi, Naka-gun, Ibaraki-ken

(Received July 30, 1987)

The equations for ideal MHD equilibria with stationary flow are re-examined and addressed as numerically applied to tokamak configurations with a free plasma boundary. Both the isothermal (purely toroidal flow) and the poloidal flow cases are treated. Experiment-relevant states with steady flow (so far only in the toroidal direction) are computed by the modified SELENE40 code.

Keywords: Ideal MHD Equilibria, Steady Flow, Free Plasma Boundary,  
Tokamak, SELENE40

---

\* Permanent Address: Max-Planck-Institut für Plasmaphysik, 8046  
Garching bei München, Federal Republic of Germany

定常流をもつトカマク平衡の数値計算

日本原子力研究所那珂研究所核融合研究部

Wolfgang KERNER\*・徳田 伸二

(1987年7月30日受理)

定常流をもつ理想MHD平衡を表わす方程式を再吟味し、自由プラズマ境界をもつトカマク配位の問題を数値的に扱った。等温的な(トロイダル流のみ)場合とポロイダル流のある場合の両方について論じる。実験に関連した定常流のある状態(ただし、現在のところ、その方向はトロイダル方向に限られる)を修正SELENE 40 コードで求めることができる。

---

那珂研究所：〒311-02 茨城県那珂郡那珂町大字向山801-1

\* マックス・プランク・プラズマ物理学研究所

(IPP, Garcking, FRG)

## Contents

1. Introduction .....	1
2. Physical model .....	3
3. Numerical scheme .....	8
3.1 Purely Toroidal Flow .....	8
3.2 General Flow .....	10
4. Results .....	14
5. Conclusions .....	17
Acknowledgements .....	18
References .....	19

## 目 次

1. 序論 .....	1
2. 物理モデル .....	3
3. 数値計算法 .....	8
3. 1 トロイダル流のみの場合 .....	8
3. 2 一般的な流れの場合 .....	10
4. 数値計算結果 .....	14
5. 結論 .....	17
謝 辞 .....	18
参考文献 .....	19

## 1. Introduction

At present controlled thermonuclear fusion research is close to demonstrating the feasibility of a fusion reactor. Three large tokamak devices, TFTR, JET, and JT-60, aim at break-even. These experiments are diagnosed and controlled by utilizing codes which are based on various plasma models. Macroscopic models describing equilibrium, stability and transport are among the most important ones. Neglecting flow and assuming isotropic pressure yields the well-known Grad-Schlüter-Shafranov equation. Ideal MHD stability of these configurations is considered a necessary condition for successful operation of a tokamak. Most transport models also neglect flow in the basic equilibrium. However, to achieve adequate simulation, the flows should be taken into account. That flows are present can be seen from the definition of the current in the two-fluid model,  $j = en(v^i - v^e) = -enu$  ( $n$ : being the density and  $v$ : the velocity). Furthermore, dissipative models require a flow for toroidal equilibria. Pfirsch-Schlüter diffusion sustains such a pressure-driven flow. If viscosity is included, the neoclassical flows nearly follow the observed behaviour. Heating power in the form of neutral-beam injection substantially increases the plasma temperature. Depending mainly on the injection angle, this beam injection generates a flow in both the toroidal and the poloidal directions. The toroidal flow velocities can become quite large, i.e. up to ion sound speed. The magnitude of the poloidal flow is still not accurately determined. Poloidal flow is most likely damped out, thereby increasing transport. This often leads to deterioration of confinement.

Although the concept of ideal MHD equilibria with flow was outlined long ago, it has not yet become a standard tool for interpreting experiments. Only recently have efforts been made to study such configurations quantitatively. Owing to the high cost of new experiments it is desirable to include such models in the design phase. In this paper we concentrate on equilibria with flow. The inertia term

$\rho \underline{u} \cdot \nabla \underline{u}$  has to be taken into account in the momentum balance. For general flow the temperature and density are no longer constant on a flux surface. More accurate measurements will substantiate this poloidal asymmetry, which can then be taken into account for stability and transport calculations.

So far only equilibria with a fixed boundary have been reported. Here the flows are built into the computation of configurations defined by experimental and engineering needs, i.e. free surface equilibria. Instead of applying the finite-element method, the finite-difference scheme on a Cartesian grid is implemented. This allows high computational efficiency. However, the inclusion of poloidal flow substantially complicates the partial differential equation. As a consequence, the very fast solvers cannot be used any more. The highly nonlinear equations are solved iteratively. Solutions for parameters within certain ranges are achieved by applying a continuation method.

The paper is organized as follows: the physical model and the equilibrium equations are derived and discussed in Section 2. Section 3 describes the numerical scheme for purely toroidal and for general flows. Both approaches are pursued. The results are presented in Section 4. The discussion and conclusion are given in Section 5.

## 2. Physical model

We begin with the ideal single-fluid MHD equations for the density  $\rho$ , the velocity  $u$ , the scalar pressure  $p$  and the magnetic field  $B$ :

$$\text{continuity: } \frac{\partial}{\partial t} \rho + \nabla \cdot (\rho u) = 0, \quad (1)$$

$$\text{momentum: } \rho \left( \frac{\partial}{\partial t} + u \cdot \nabla \right) u = -\nabla p + j \times B, \quad (2)$$

$$\text{Maxwell-Ohm: } \frac{\partial}{\partial t} B = \nabla \times (u \times B), \quad (3)$$

$$\text{Maxwell: } \nabla \cdot B = 0, \quad (4)$$

$$j = \nabla \times B. \quad (5)$$

The absence of any dissipation is expressed by the conservation of the entropy  $S$  :

$$\left( \frac{\partial}{\partial t} + u \cdot \nabla \right) S = 0. \quad (6)$$

The plasma is assumed to be an ideal gas, i.e.

$$p = T \rho, \quad (7)$$

$T$  being the temperature. The thermodynamic relations lead to the caloric equation of state [ 1 ] :

$$p = S \rho^\gamma, \quad (7a)$$

where  $\gamma$  is the ratio of the specific heats, which is taken as equal to 5/3, as usual. A macroscopic model incorporating dissipation as well as flow (see Kerner and Weitzner [2,3] and references therein) shows that static equilibria and those with purely toroidal flow conserve entropy. Furthermore, the temperature is constant along  $B$ , i.e. constant on a flux surface. In next order in a small expansion parameter  $\epsilon$  there is poloidal flow, but this flow is within a magnetic surface, and the temperature varies on a magnetic surface. In second order in  $\epsilon$  perpendicular mass and energy transport occurs. Hence our flow model should incorporate isotropic temperature, i.e.  $T = T(\Psi)$  ( $\Psi$  : being the poloidal flux), in conjunction with purely toroidal flow and anisotropic temperature when poloidal



flow is included. This poloidal flow, although small, is strongly coupled with enhanced radial transport.

To compute axisymmetric equilibria, we work in the usual cylindrical coordinates  $r, \theta, z$ , with  $\theta$  being the ignorable coordinate. The stationary, i.e.  $\partial/\partial t=0$ , equations read

$$\nabla(\rho u) = 0, \quad (8)$$

$$\rho(u \cdot \nabla)u = -\nabla p + (\nabla \times B) \times B, \quad (9)$$

$$\nabla \times (u \times B) = 0, \quad (10)$$

$$\nabla \cdot B = 0, \quad (11)$$

$$(u \cdot \nabla)S = 0, \quad (12)$$

$$p = S\rho^{\gamma}. \quad (13)$$

The equations for equilibria with flow were first derived by Zehrfeld and Green [4]. Here we closely follow a more recent derivation by Hameiri [5,6] used in the finite-element code of Kerner and Jandl [7].

The magnetic field is represented as

$$B = \nabla \theta \times \nabla \psi + F \nabla \theta, \quad (14)$$

where  $\psi$  is the poloidal flux and  $F$  the poloidal current profile. The continuity equation is satisfied by

$$\rho u = \nabla \theta \times \nabla \lambda + \rho \Lambda \nabla \theta. \quad (15)$$

The Maxwell-Ohm equation

$$\nabla \times (u \times B) = 0$$

implies the existence of an electric potential  $u \times B = \nabla \varphi$ . The projection along  $B$  yields  $\varphi = \varphi(\psi)$ , the  $\theta$ -component  $u \cdot \nabla \psi = 0$  and hence  $\lambda = \lambda(\psi)$  and eventually the  $\psi$ -component,

$$\varphi' = -\frac{\Lambda}{r^2} + \frac{F\lambda'}{\rho r^2}, \quad (16)$$

where the prime denotes the derivative with respect to the argument, i.e.

$$\varphi' = \frac{d\varphi}{d\psi}.$$

Introducing  $\Omega = \varphi'$  and  $\Phi = \lambda'$ , we obtain for the velocity the representation

$$u = \frac{\Phi(\psi)}{\rho} B + r^2 \Omega(\psi) \nabla \theta. \quad (17)$$

The flow is within a magnetic surface and may have a toroidal component. One consequence of this is that  $T = T(\psi)$  in the toroidal flow case, otherwise  $S = S(\psi)$ .

We then recover the usual adiabatic equation

$$\frac{d}{dt}(P/\rho^\gamma) = \frac{d}{dt}S = 0.$$

The  $\theta$ -component of the momentum equations causes the component of the velocity and the field to be restricted by the identity

$$F = [I(\psi) + \Phi \Omega / |\nabla \theta|^2] / (1 - \Phi^2 / \rho), \quad (18)$$

where  $I = I(\psi)$  is a surface quantity. In the case with no poloidal flow, i.e.  $\Phi = 0$ , this identity gives  $F = F(\psi)$ . The projection along  $B$  gives

$$H(\psi) = \frac{\Phi^2}{2\rho^2} B^2 - \frac{\Omega^2}{2|\nabla \theta|^2} + \frac{\gamma}{\gamma-1} S(\psi) \rho^{\gamma-1}, \quad (19)$$

where  $H = H(\psi)$  is a free surface quantity. For  $T = T(\psi)$  the third term on the right hand side is replaced by  $T \ln \rho$ . The  $\nabla \psi$ -component of the momentum equation yields

$$\nabla \left[ \left(1 - \frac{\Phi^2}{\rho}\right) r^{-2} \nabla \Phi \right] + u \cdot B \frac{d\Phi}{d\psi} + \rho \left( -\frac{\Omega}{|\nabla \theta|^2} + \frac{F\Phi}{\rho} \right) \frac{d\Omega}{d\psi} + |\nabla \theta|^2 r \frac{dI}{d\psi} + \rho \frac{dH}{d\psi} - \frac{1}{\gamma-1} \rho^\gamma \frac{dS}{d\psi} = 0, \quad (20)$$

inside the plasma, where the entropy term is replaced by

$$-(\ln \rho - 1) \rho \frac{dT}{d\psi}$$

if the temperature is constant on a magnetic surface, and

$$\nabla \cdot (r^{-2} \nabla \psi) = 0 \quad (21)$$

in the surrounding vacuum. The shape of the plasma surface is specified. The vacuum solution for the poloidal flux supplied by external coils together with general vacuum solutions are used to control the plasma shape in the way described in Refs. [8,9]. Together with the plasma cross-section we can specify the five

surface functions  $\Phi, \Omega, I, H$  and  $S$ . The functions  $F$  and  $\rho$  are, in general, not surface quantities. Together with the partial differential equations (20,21) the two algebraic equations (17) and (18) have to be satisfied. Equation (19) contains the information that  $\rho$  is a function of  $|\nabla\psi|^2$ . To be more precise, one has

$$\rho = \rho(r, \psi, |\nabla\psi|^2). \quad (22)$$

Closer inspection of the differential equation (20) reveals that the type of the equation is defined by the second derivatives, i.e. by the term

$$\nabla[(1-\Phi^2/\rho)|\nabla\psi|^2\nabla\psi]. \quad (23)$$

Using the relation (22), it is seen that the highest derivatives are due to

$$(1-\Phi^2/\rho)\Delta\psi + (\Phi^2/\rho^2)\nabla\psi \cdot \nabla\rho,$$

where

$$\nabla\psi \cdot \nabla\rho = \frac{\partial\rho}{\partial r} \nabla\psi \cdot \nabla r + \frac{\partial\rho}{\partial\psi} \nabla\psi \cdot \nabla\psi + \frac{\partial\rho}{\partial|\nabla\psi|^2} \nabla\psi \cdot \nabla|\nabla\psi|^2.$$

It is convenient to normalize the velocity along  $B$  (poloidal component) to the poloidal Alfvén velocity

$$A = \Phi / \sqrt{\rho}. \quad (24)$$

We introduce the notation

$$\dot{\rho} = \frac{\partial\rho}{\partial|\nabla\psi|^2}, \quad (25)$$

$$\alpha = 2A^2 \dot{\rho} / \rho \quad (26)$$

and obtain for the terms with second derivatives  $(1-A^2)\Delta\psi + 1/2\alpha\nabla\psi \cdot \nabla|\nabla\psi|^2$  or, in more detail,

$$(1-A^2 + \alpha\psi^2_{,r})\psi_{,rr} + 2\alpha\psi_{,r}\psi_{,z}\psi_{,rz} + (1-A^2 + \alpha\psi^2_{,z})\psi_{,zz}. \quad (27)$$

As shown in Refs. [4,5], the quasilinear partial differential equation (20) is elliptical if

$$0 \leq A^2 \leq \beta, \quad (28)$$

where the plasma beta is defined as  $\beta = \gamma p / (\gamma p + B^2)$ . Since the transport estimates

given above imply small poloidal flow, we shall not be concerned with flows in the hyperbolic domain  $A^2 > \beta$ . For small poloidal flow velocities satisfying eq. (28) the differential equation (20) is strictly elliptic. There are then no additional difficulties in solving the algebraic equations (18) and (19), as can be seen from the theory of implicit functions. Care must be taken, however, that the choice of the free functions does not restrict the solvability. The entropy  $S$  especially is an unusual profile function. It is therefore eliminated by the transformation used in Ref. [6] :

$$\tilde{\rho} = S^{1/\gamma} \rho, \quad \tilde{\Omega} = S^{-1/2\gamma} \Omega, \quad \tilde{\Phi} = S^{1/2\gamma} \Phi. \quad (29)$$

The equations using the fact that  $\tilde{B} = B$ ,  $\tilde{u} = S^{-1/2\gamma} u$  and  $\tilde{H} = HS^{-1/\gamma}$  read

$$F = (I + \tilde{\Omega} \tilde{\Phi} / |\nabla \theta|^2) / (1 - \tilde{\Phi}^2 / \tilde{\rho}), \quad (18b)$$

$$\tilde{H} = \frac{\tilde{\Phi}^2}{2\tilde{\rho}^2} B^2 - \frac{\tilde{\Omega}^2}{2|\nabla \theta|^2} + \frac{\gamma}{\gamma-1} \tilde{\rho}^{\gamma-1}, \quad (19b)$$

$$\nabla \left[ \left( 1 - \frac{\tilde{\Phi}^2}{\tilde{\rho}} \right) |\nabla \theta|^2 \nabla \psi \right] + \tilde{u} \cdot B \frac{d\tilde{\Phi}}{d\psi} + \tilde{\rho} \left( \frac{\tilde{\Omega}}{|\nabla \theta|^2} + \frac{F\tilde{\Phi}}{\tilde{\rho}} \right) \frac{d\tilde{\Omega}}{d\psi} + |\nabla \theta|^2 F \frac{dI}{d\psi} + \tilde{\rho} \frac{d\tilde{H}}{d\psi} = 0. \quad (20b)$$

A solution of eqs. (18b) - (20b), i.e.  $S=1$ , together with four arbitrary functions  $\tilde{\Phi}, \tilde{\Omega}, I$  and  $\tilde{H}$  generates with the transformation (29) a family of new equilibria with profiles  $S=S(\psi)$ .

### 3. Numerical scheme

#### 3.1 Purely Toroidal Flow

Owing to the level of complication, the solutions for purely toroidal and for general flow are treated separately.

The temperature is a surface quantity, i.e.  $T=T(\psi)$  is used instead of the entropy. The pressure is then given by  $p=T(\psi)\rho$ . For zero poloidal flow  $\phi=0$  eq. (18) gives  $F=F(\psi)$ . The Bernoulli-type equation (19) reads

$$H(\psi) = -\frac{\Omega^2(\psi)}{2|\nabla\theta|^2} + T(\psi) \ln \rho.$$

If we introduce

$$H_0 = \frac{H}{T} + \ln T \quad \text{and} \quad \Omega_0 = \frac{\Omega}{\sqrt{T}}, \quad (30)$$

we obtain

$$H_0(\psi) + \frac{\Omega_0^2}{2|\nabla\theta|^2} = \ln p$$

and further

$$p = \exp(H_0 + \Omega_0^2/2|\nabla\theta|^2). \quad (31)$$

The differential equation reads

$$\nabla[|\nabla\theta|^2 \nabla\psi] + |\nabla\theta|^2 F \frac{dF}{d\psi} + p \left[ \frac{\Omega_0}{|\nabla\theta|^2} \frac{d\Omega_0}{d\psi} + \frac{dH_0}{d\psi} \right] = 0 \quad (32)$$

or

$$\nabla[|\nabla\theta|^2 \nabla\psi] + |\nabla\theta|^2 F \frac{dF}{d\psi} + \frac{\partial p}{\partial \psi} = 0.$$

This equation together with the vacuum equation has the form of the Grad-Schlüter-Shafranov equation with arbitrary profiles  $F, \Omega_0, H_0$  and a free function  $T=T(\psi)$  in the transformation (30). We normalize the flow velocity to the ion sound speed

$$v_s^2 = \gamma p / \rho = T \quad (\text{here } \gamma=1) \quad (33)$$

and obtain for the normalized toroidal flow

$$\hat{v}_t = \frac{v_\theta}{v_s} = \bar{r} \quad \Omega_0 R_N, \quad (\bar{r} = \frac{r}{R_N})$$

where the normalization length  $R_N$  is chosen as the radius of the magnetic axis,  $R_N=R_a$ . For a given profile  $\hat{v}_t$  the function  $\Omega_0$  is then

$$\Omega_0 = \hat{v}_t / R_a. \quad (34)$$

We further define

$$P_0 = e^{H_0}$$

and get

$$P = P_0(\psi) e^{1/2 r^2 \Omega_0^2} \quad (35)$$

For a specified plasma shape the equilibrium has to satisfy

$$\nabla(\nabla\psi/r^2) = -R \frac{dF}{d\psi} / r^2 - \frac{\partial p}{\partial \psi} = g \quad \text{in the plasma domain } \Gamma \quad (36.a)$$

$$\nabla(\nabla\psi/r^2) = 0 \quad \text{in the vacuum with } \psi = ct. \text{ on } \partial\Gamma. \quad (36.b)$$

The equations are solved in a rectangular domain where the currents in external coils are adjusted to satisfy  $\psi = \psi_s$  on  $\partial\Gamma$  at given (here five) fixed points. The system (36) is nonlinear and hence an iteration method has to be used. Here the usual Piccard iteration is applied. To avoid the trivial solution  $\psi = 0$ , an eigenvalue is introduced. The numerical scheme is then

$$\nabla(\nabla\psi^n/r^2) = \lambda^{n-1} g(r, \bar{\psi}^{n-1}) \quad \text{in plasma} \quad (37.a)$$

$$\nabla(\nabla\psi^n/r^2) = 0 \quad \text{in vacuum} \quad (37.b)$$

$$\psi = \psi_s \quad \text{on } \partial\Gamma, \quad (37.c)$$

where the profile functions in the inhomogeneous term  $g$  are given as a function of the normalized flux  $\bar{\psi}$ ,  $\bar{\psi} = (\psi - \psi_s) / (\psi_0 - \psi_s)$ , with  $\psi_s, \psi_0$  the poloidal flux on the surface and axis, respectively ( $\psi_s = 0$ ). The system (37) is solved numerically in a rectangular domain by using the double-cyclic reduction method [10]. The eigenvalue  $\lambda$  is determined at the  $n$ -th step by  $\lambda^{n-1} = (\psi_0 / \psi_0^{n-1}) \lambda^{n-2}$ , where the value of  $\psi_0$  is obtained by the constraint that either the total toroidal current or the toroidal current on axis, this being equivalent to specifying the safety

factor on axis  $q_0$ , match a given value. The iteration converges when the change is smaller than a prescribed tolerance, i.e.  $|\lambda^n - \lambda^{n-1}|/\lambda^n < \epsilon$  and  $\|\psi^n - \psi^{n-1}\| < \epsilon$ .

The equilibrium with flow is computed by a continuation method using a parameter  $\alpha_t$ ,  $0 \leq \alpha_t \leq 1$ . A static equilibrium is started with and the flow is added in steps  $\Omega^* = \alpha_t \Omega_0$  with  $\alpha_t \rightarrow 1$ .

### 3.2 General Flow

For poloidal flow the temperature is no longer a surface quantity and the caloric equation  $P = S\rho^\gamma$  has to be used. The density  $\rho$  has also poloidal dependence and has to be determined numerically from eq. (19b), whereas the poloidal current function  $F$  is merely replaced according to eq. (18b). It is obvious that an improper choice of the shape and the profile functions  $\hat{\phi}, \hat{\Omega}, \hat{H}$  and  $\hat{I}$  will considerably restrict the numerical solution for  $\hat{\rho}$ . Let us introduce normalized quantities, using the sound velocity, eq. (33), and the Alfvén velocity

$$v_A^2 = B^2 / \rho, \quad (38)$$

$$\hat{u}_B = \frac{u_B}{v_a} = \frac{\Phi / \rho B}{B / \sqrt{\rho}} = A, \quad (39)$$

$$\hat{u}_\theta = \frac{u_\theta}{v_s} = \frac{\bar{r} R_N \hat{\Omega}}{\sqrt{\gamma \rho^{\gamma-1}}}. \quad (40)$$

Note that

$$P = \hat{\rho}^\gamma. \quad (41)$$

To make the connection to experimental data clearer, we introduce a reference line in the plane  $z=0$  based on a nested set of magnetic surfaces with the value  $\psi_0$  on axis and  $\psi_s$  on the plasma surface following Semenzato et al. [11]:

$$C_R = \left\{ r, z : r = r_R(\psi), z = z_R(\psi) = 0 ; \psi \in [\psi_0, \psi_s] \right\}. \quad (42)$$

A profile function  $f$  can then be defined by

$$f_R(\psi) = f(r_R(\psi), z_R(\psi)) \quad (43)$$

and in dimensionless form if  $f_R \neq 0$

$$\bar{f} = f(r, z) / f_R. \quad (44)$$

The pressure is a profile function well studied in  $\beta$ -optimization computations. A maximum value can be obtained by evaluating the ideal ballooning mode equation for every magnetic surface as was done by Tsunematsu et al. [9]. Since neutral beam heated plasmas cannot exceed the ideal MHD stability  $\beta$ -limit,  $P_R$  is obviously as one of our profile functions, which then fixes  $\tilde{\rho}_R = P_R^{1/\gamma}$ . From eq. (19b) we obtain for the pressure

$$P = (\tilde{\rho} \tilde{H} - 1/2 \tilde{\Phi}^2 / \tilde{\rho} B^2 + 1/2 \tilde{\rho} r^2 \tilde{\Omega}^2) \frac{(\gamma-1)}{\gamma}. \quad (45)$$

From the deposition profiles for the neutral beams one can get estimates for the poloidal and toroidal flows  $\hat{u}_B$  and  $\hat{u}_\theta$ , from which  $\tilde{\Phi}$  and  $\tilde{\Omega}$  are evaluated :

$$\tilde{\Phi} = (\hat{u}_B)_R \sqrt{\tilde{\rho}_R}, \quad (46)$$

$$\tilde{\Omega} = (\hat{u}_\theta)_R \gamma^{1/2} \tilde{\rho}^{(\gamma-1)/2} R / R_R. \quad (47)$$

The remaining input functions are chosen by the values of  $\hat{H}$  and  $F$  on the reference line

$$\hat{H} = \frac{1}{2} (\hat{u}_B)_R^2 (v_a)_R^2 + (v_s)_R^2 \left[ \frac{1}{\gamma-1} - \frac{1}{2} (\hat{u}_\theta)_R^2 \right] \quad (48)$$

and with given  $F_R$ , from which the function  $I$  is then obtained ,

$$F_R = \frac{I + R_R (\hat{u}_\theta)_R (\hat{u}_B)_R (\gamma P_R)^{1/2}}{1 - (\hat{u}_B)_R^2} = \frac{I + K_R}{1 - (\hat{u}_B)_R^2},$$

the equation for  $F$  in dimensionless form is

$$\bar{F} = \frac{I + \bar{r}^2 K_R}{I + K_R}. \quad (49)$$

The remaining algebraic equation for  $\tilde{\rho}$  then yields



$$2\tilde{\rho}^2(\tilde{\rho}^{\gamma-1}-1)/(\gamma-1)=2\tilde{\rho}^2\left[\langle\hat{u}_B\rangle_R^2\left(\frac{v_A}{v_S}\right)_R^2+\langle\hat{u}_\theta\rangle_R^2(\bar{r}^2-1)\right]-\langle\hat{u}_B\rangle_R^2\left(\frac{v_A}{v_S}\right)^2 B^{-2}. \quad (50)$$

Let us now consider the case of purely toroidal flow, where

$$\tilde{\rho}^{\gamma-1}=\langle\hat{u}_\theta\rangle_R^2(\bar{r}^2-1)(\gamma-1)+1.$$

For the plasma shapes with up-down symmetry considered here we obtain on the reference line  $\bar{r}^2 \geq 1$  and hence the algebraic relation can be solved for  $\tilde{\rho}$ . Since the toroidal flow is not further restricted, an improper choice of the reference line may yield negative values too large for  $\bar{r}^2-1$ , allowing no real roots for  $\tilde{\rho}$ ! It is also obvious that eq.(50) can be solved for  $\tilde{\rho}$  when the condition for ellipticity is satisfied, i.e.  $A^2 \leq \beta$ . The plasma boundary is a surface of zero pressure and hence  $\tilde{\phi}$  and  $\tilde{Q}$  must also vanish there. When  $k$  is defined as  $k=(1-\tilde{\phi}^2/\tilde{\rho})/r^2$  and the remaining terms in eq.(20b) by  $G$ , the system to be solved eventually takes the form

$$r^2 \nabla(k \nabla \psi) = G(r, z) \quad \text{in } \Gamma \quad (51.a)$$

$$r^2 \nabla(\nabla \psi / r^2) = 0 \quad \text{in vacuum} \quad (51.b)$$

with

$$\psi = ct \quad \text{on } \partial\Gamma. \quad (51.c)$$

This nonlinear equation is again solved by iteration. The first solution was obtained by applying the finite-element method; see Kerner, Jandl [7] and Semenzato et al. [11]. The Piccard iteration used in both cases is

$$r^2 \nabla(k(\psi^{n-1}) \nabla \psi^n) = \lambda^{n-1} G(r, z, \psi^{n-1}). \quad (52)$$

As discussed above, the second-order derivatives are not consistently treated. Here we apply finite differences based on eq.(27). The divergence term in eq.(51) is then approximated by

$$a(\psi^n) \psi_{,rr}^{n+1} + b(\psi^n) \psi_{,rz}^{n+1} + c(\psi^n) \psi_{,zz}^{n+1} - (1-A^2) \psi_{,r}^{n+1} / r = G(r, z, \psi^n), \quad (52')$$

where

$$a=1-A^2+a\psi_{,r}^2,$$

$$b=2\alpha\psi_{,r}\psi_{,z},$$

$$c=1-A^2+\alpha\psi_{,z}^2,$$

$$\alpha=\frac{A^2/r^2}{B_p^2+B_t^2/(1-A^2)-\gamma p/A^2},$$

with

$$A^2=\tilde{\phi}^2/\bar{\rho}=(u_D)^2_R/\bar{\rho}$$

and

$$p=\bar{\rho}^r p_R.$$

For zero parallel flow, i.e.  $A=0$ , the usual  $\Delta^*$  operator is recovered. The fact that  $a, b$  and  $c$  are different functions of  $r$  and  $z$  prohibits the use of the fast double-cyclic reduction method implemented for toroidal flow. The rather artificial operator splitting in the form of Refs. [7,11],

$$(1-A^2)r^2\nabla(\nabla\psi/r^2)+\nabla\psi\cdot\nabla(1-A^2),$$

yielding the iteration

$$\Delta^*\psi^{n+1}=\frac{1}{1-A^2}\left[G(r,z,\psi^n-\nabla\psi^n\cdot\nabla(1-A^2))\right] \quad (53)$$

is not applied here. Centered finite differences lead to a system of linear equations with block-tridiagonal structure. This system is solved by standard block LDU decomposition. An eigenvalue  $\lambda$  is introduced in eq.(52) such that  $q_0$  assumes a prescribed value. The equilibrium with flow is again computed by using the continuation method. First the static case is solved, then toroidal flow is taken into account by increasing the parameter  $\alpha_t$  from zero to one,  $0\leq\alpha_t\leq 1$ . Finally, parallel flow is switched on by increasing the second parameter  $0\leq\alpha_p\leq 1$ . The iteration is terminated if the change in the solution  $\psi$  is smaller than a desired tolerance

$$\|\psi^n-\psi^{n-1}\|<\varepsilon \text{ or } |\lambda^n-\lambda^{n-1}|/\lambda^n<\varepsilon.$$

This procedure guarantees solution of the highly nonlinear, quasilinear differential equation for certain parameter ranges.

## 4. Results

### (A) Purely Toroidal Flow

This version of the code is suited to computing tokamak equilibria with temperature being constant on a flux surface and with poloidal flow damped out by enhanced transport. Some results have been evaluated analytically (Refs. [12,13] ) and computed numerically (Refs. [7,14,15] ). The results presented here are different since the free-boundary problem including plasma and vacuum in conjunction with external coils is solved.

To validate the code, the first application is cases treated by Kerner and Jandl [7]. The plasma-vacuum interface is defined as

$$r=R_0+a \cos[\theta+\delta \sin \theta], \quad (54)$$

$$z=K \sin \theta,$$

with up-down symmetry imposed and  $0 \leq \theta \leq \pi$ . The chosen parameters for the aspect ratio  $R_0/a=3$ , the elongation  $K=2.5$  and the triangularity  $\delta=0.45$  are difficult to match since our boundary is fixed by only five points. The resulting plasma contour is consequently different. We therefore somewhat relax the data to  $R_0/a=3$  with  $R_0=3.2$ ,  $K=2.0$  and  $\delta=0.25$ . The dependence of the solution on the mesh size is analyzed for  $K=1.0$  and  $p'=-2, FF'=+0.5 \cdot R_0^2$  and  $R_a \Omega_0'=-1.0$  with  $R_a \Omega_0=1.0$  and  $\Omega_0=0$ . Quantities relevant to the numerical accuracy are the value of the safety factor on the surface,  $q_a$ , the value of  $\psi$  on axis,  $\psi_0$ , and the position of the magnetic axis  $R_a$ . The safety factor is unity on axis,  $q_0=1.0$ . Quadratic convergence is found without and with flow, as is shown in Fig.1. The position of the magnetic axis is already determined accurately by a very coarse mesh. Such convergence is also found for other profiles. For fixed profiles  $p'=-2, FF'=-0.5 \cdot R_0^2$ ,  $R_a \Omega_0'=-1$ , and  $q_0=1.0$  the shift of magnetic axis with increasing flow velocity is plotted in Fig.2. The elongation varies from  $K=2$  to  $K=0.5$ . The shift is more pronounced as the elongation of the plasma becomes

smaller. This is in agreement with the findings of Ref. [7]. It is, however, observed that the pressure strongly increases with  $\Omega_0$  (see eq.(35)). Since the toroidal current on the axis is kept fixed, the value for beta poloidal,  $\beta_I$ , is changed, and eventually completely different (here more peaked) current profiles evolve with a smaller  $\beta$  value.

In the next application we aim at reproducing a realistic configuration with toroidal flow present. Let us first consider the equilibrium without flow, as shown in Fig.3. The pressure  $p(r, z=0)$ , the safety factor  $q(\bar{\psi})$ , the flux function  $\psi(r, z=0)$ , and the two-dimensional flux and pressure contours are displayed. The total beta is  $\beta=3.3\%$  and the poloidal beta  $\beta_I=1.5$ . Next we introduce a flow profile  $\Omega_0$  together with a pressure function  $p_0(\bar{\psi})=e^{H_0}$ , which generate the same total pressure on the line  $z=0$ . Two branches for the flow occur as shown in Fig.4, which are defined by fitting the total pressure for  $r \leq R_a$  and for  $r \geq R_a$ , respectively. When the velocity profile which increases with  $\bar{\psi}$  is chosen, high beta equilibria are generated. The profiles displayed in Fig.5 yield an equilibrium with  $\beta=6.4\%$  and  $\beta_I=1.40$  and those displayed in Fig.6, one with  $\beta \sim 9\%$  and  $\beta_I=1.24$ . Clearly the total pressure and current profiles become broader. The shift of the pressure maximum becomes more pronounced than the shift of the magnetic axis. Since the flow is larger outside the plasma, the temperature and the safety factor become hollow in the centre. Hollow discharges are therefore caused not only by impurity accumulation at the centre but also by beam deposition localized near the plasma edge. These equilibria will certainly have unfavourable stability behaviour. It is quite unlikely that the flow maximum near the plasma edge will be sustained for a long time. More likely the discharge will quickly decay. When the neutral-beam energy is deposited mainly at the centre of the plasma, velocity profiles such as displayed in Fig.7 develop. In this case the toroidal flow and also its derivative vanish at the wall. For mass flow with

maximum velocity of half the second speed,  $\hat{v}_t \approx 0.5$ , the equilibrium shown in Fig.7 is obtained. The  $\beta$  values are  $\beta = 5.3\%$  and  $\beta_I = 1.7$ . A class of equilibria can be generated with the same global properties, differing only in the flow profile. This implies quite different  $\Omega_0'$  profiles. This property can be used to monitor the slope of the safety factor or of the toroidal current locally. Thereby, the stability of localized ideal MHD modes (ballooning modes) may be favourably influenced. This may allow improvement of the performance of neutral-beam-heated tokamaks towards higher beta values.

## 5. Conclusions

Tokamak devices aiming at break-even are becoming quite costly owing to the large plasma volume and the large amount of additional heating required. Realistic simulation of tokamak plasmas is therefore becoming essential. The macroscopic behaviour of the toroidal configuration has to be studied quantitatively. Static equilibria evaluated by numerically solving the Grad-Schlüter equation provide knowledge about the magnetic surfaces. At high plasma pressure, however, the simulation of the pressure and the density becomes poor since the poloidal asymmetry of these quantities is neglected. More refined models are becoming necessary. Especially in the case of substantial neutral-beam heating, the flow of the plasma should be taken into account. Two such models are presented here. The first model assumes the temperature to be constant on a flux surface and is suited to simulation when the poloidal rotation is damped out by enhanced transport. This model does not introduce additional difficulties for its numerical solution. We have computed realistic, high-beta equilibria. If the injection generates maximum flow at the outside of the plasma, discharges with hollow profiles occur. On the other hand, profiles with the maximum flow velocity inside the plasma yield smooth equilibria. The free profile functions can be adjusted to reproduce measured data such as density and pressure. The contours of constant pressure do not coincide with those of constant poloidal flux. The variation of pressure and density on a flux surface is of the order of the inverse aspect ratio. Naturally, it also depends on the flow velocity.

It is observed that the current and safety factor can be changed locally while keeping the global properties of the configuration constant. Neutral-beam-heated equilibria with flow can thus have improved stability properties, especially with respect to the ballooning and tearing modes. For zero mass flow the linearized ideal MHD equations yield a self-adjoint operator for the stability analysis.

The energy principle utilizes this property as well as the numerical schemes. For finite flow the stability operator is no longer self-adjoint. The stability analysis therefore becomes considerably more involved, especially for toroidal geometry. So far only the effect of rigid toroidal rotation on ideal ballooning modes has been studied (Refs. [6,16] ). The equilibrium flow can lead to an unstable continuous spectrum (Refs. [17,18] ). One therefore has to expect additional instabilities, which may counteract the stabilizing effect on localized, static modes. In some cases, however, these new instabilities may have only small growth rates and may not be essential.

In the second model the poloidal flow is kept finite, yielding a poloidal dependence for the temperature. The resulting quasilinear differential equation has different properties compared with the static case. Only for small poloidal flow is the equation elliptic. The numerical scheme proposed in the paper is different from the finite-element method used earlier. Thus, our method will substantially differ in the iteration scheme. We intend to implement this version soon. In our opinion, equilibria with flow should be used in transport simulation. Especially, the poloidal asymmetry of density and pressure is essential for correct understanding. In addition, the finite flow may substantially change the radial transport.

#### Acknowledgement

The authors are grateful to Dr.Takeda and Dr.Tsunematsu for interesting suggestions and discussions. One of the authors (W.K.) would like to express gratitude to JAERI for inviting him and its kind hospitality during his stay there. He also acknowledges the Theory Division in the Department of Thermonuclear Fusion Research for its friendly and stimulating working atmosphere.

The energy principle utilizes this property as well as the numerical schemes. For finite flow the stability operator is no longer self-adjoint. The stability analysis therefore becomes considerably more involved, especially for toroidal geometry. So far only the effect of rigid toroidal rotation on ideal ballooning modes has been studied (Refs. [6,16] ). The equilibrium flow can lead to an unstable continuous spectrum (Refs. [17,18] ). One therefore has to expect additional instabilities, which may counteract the stabilizing effect on localized, static modes. In some cases, however, these new instabilities may have only small growth rates and may not be essential.

In the second model the poloidal flow is kept finite, yielding a poloidal dependence for the temperature. The resulting quasilinear differential equation has different properties compared with the static case. Only for small poloidal flow is the equation elliptic. The numerical scheme proposed in the paper is different from the finite-element method used earlier. Thus, our method will substantially differ in the iteration scheme. We intend to implement this version soon. In our opinion, equilibria with flow should be used in transport simulation. Especially, the poloidal asymmetry of density and pressure is essential for correct understanding. In addition, the finite flow may substantially change the radial transport.

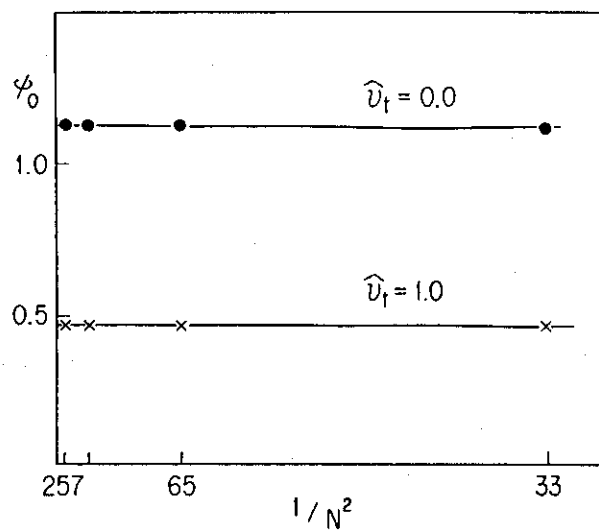
#### Acknowledgement

The authors are grateful to Dr.Takeda and Dr.Tsunematsu for interesting suggestions and discussions. One of the authors (W.K.) would like to express gratitude to JAERI for inviting him and its kind hospitality during his stay there. He also acknowledges the Theory Division in the Department of Thermonuclear Fusion Research for its friendly and stimulating working atmosphere.

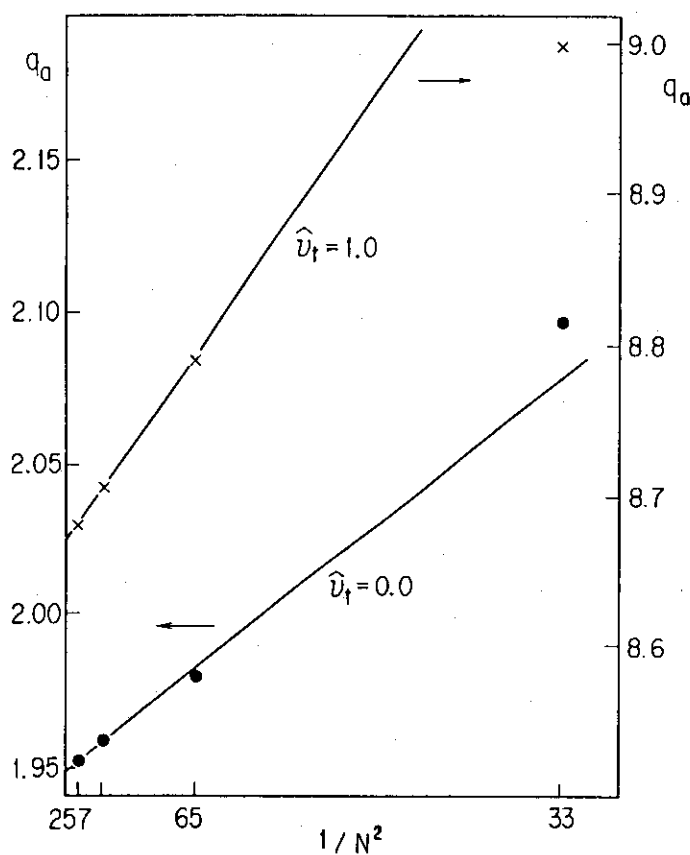


# References

- [1 ] R. Courant and K.O. Friedrichs, in *Supersonic Flow and Shock Waves*, vol. 1 (Interscience, New York, 1948).
- [2 ] W. Kerner, H. Weitzner, *Comp.Phys.Comm.* **31**(1984) 249.
- [3 ] W. Kerner, H. Weitzner, Courant Institute Report MF-107 ( DOE/ER/03077-269 ), December 1985.
- [4 ] H.P. Zehrfeld and B.J. Green, *Nucl. Fusion* **10**(1970) 251 and **12**(1972) 569.
- [5 ] E. Hameiri, *Phys.Fluids* **26**(1983) 230.
- [6 ] E. Hameiri, *Phys. Rev. A* **27**(1983) 1259.
- [7 ] W. Kerner, O. Jandl, *Comp.Phys.Comm.* **31**(1984) 269.
- [8 ] K. Lackner, *Comput. Phys. Commun.* **12**(1976) 33.
- [9 ] T. Tsunematsu, S. Tokuda , T. Nemoto, M. Azumi and T. Takeda, Japan Atomic Energy Research Institute Report JAERI-M 86-172, November 1986.
- [10] R.W. Hockney, in *Methods in Computational Physics* Vol.9 (Academic Press, New York 1970) 135.
- [11] S. Semenzato, R. Gruber and H.P. Zehrfeld, *Comp. Phys. Rep.* **1**(1984) 389.
- [12] E.K. Maschke and H. Perrin, *Plasma Phys.* **22**(1980) 579.
- [13] K. Elsässer and A. Heimsoth , *Z. Naturforschung A* **41a**(1986) 883.
- [14] L.L. Lao, *Comput.Phys.Comm.* **31**(1984) 201.
- [15] W.A. Cooper and S.P. Hirshman, Lausanne Report LRP 299/86 , March 1987.
- [16] E. Hameiri and P. Laurence, *J. Math. Phys.* **25**(1984) 396.
- [17] T.A.K. Hellsten and G.O. Spies, *Phys. Fluids* **22** (1979) 743.
- [18] E. Hameiri and J.H. Hammer, *Phys. Fluids* **22** (1979) 1700.



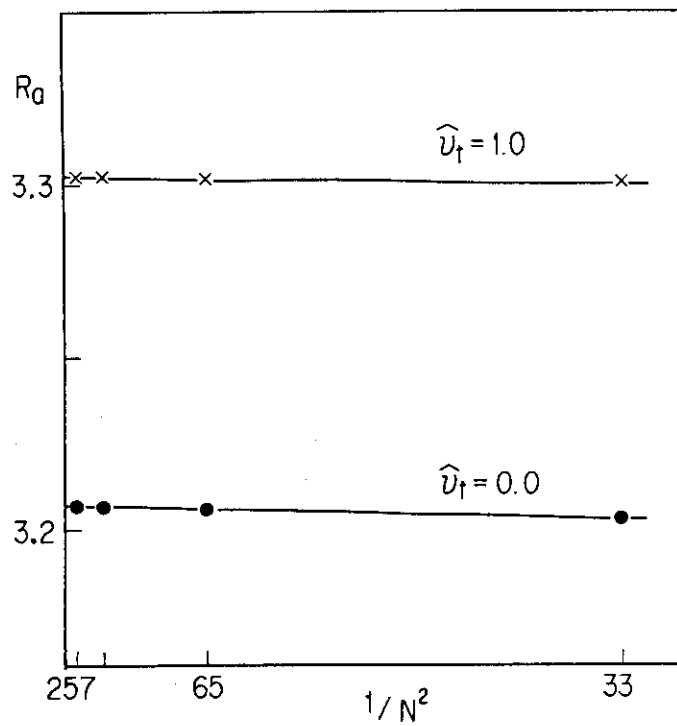
(a)



(b)

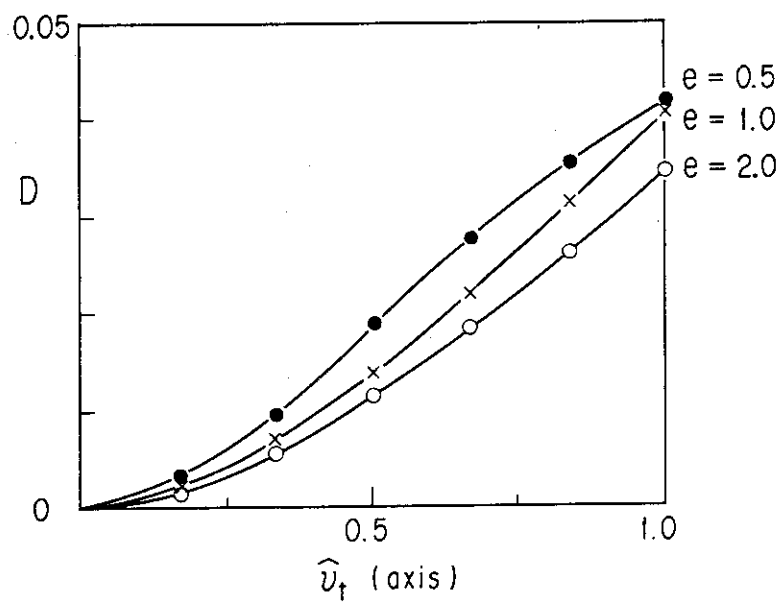
Fig.1 Convergence study: The dependence of relevant parameters on the mesh size is displayed, i.e the number of radial grid points  $N=NR=2NZ$  is indicated.

- a) The poloidal flux on axis  $\psi_0$  for zero and unity flow on axis  $\hat{v}_t=0$  and 1.  
 b) The safety factor on surface  $q_a$  for zero and unity flow on axis  $\hat{v}_t=0$  and 1.  
 c) The position of the magnetic axis for zero and unity flow on axis  $\hat{v}_t=0$  and 1.



(c)

Fig. 1 (continue)

Fig.2 Shift of the magnetic axis  $D=R_a(\vartheta)/R_a(0)-1$  with increasing flow velocity.

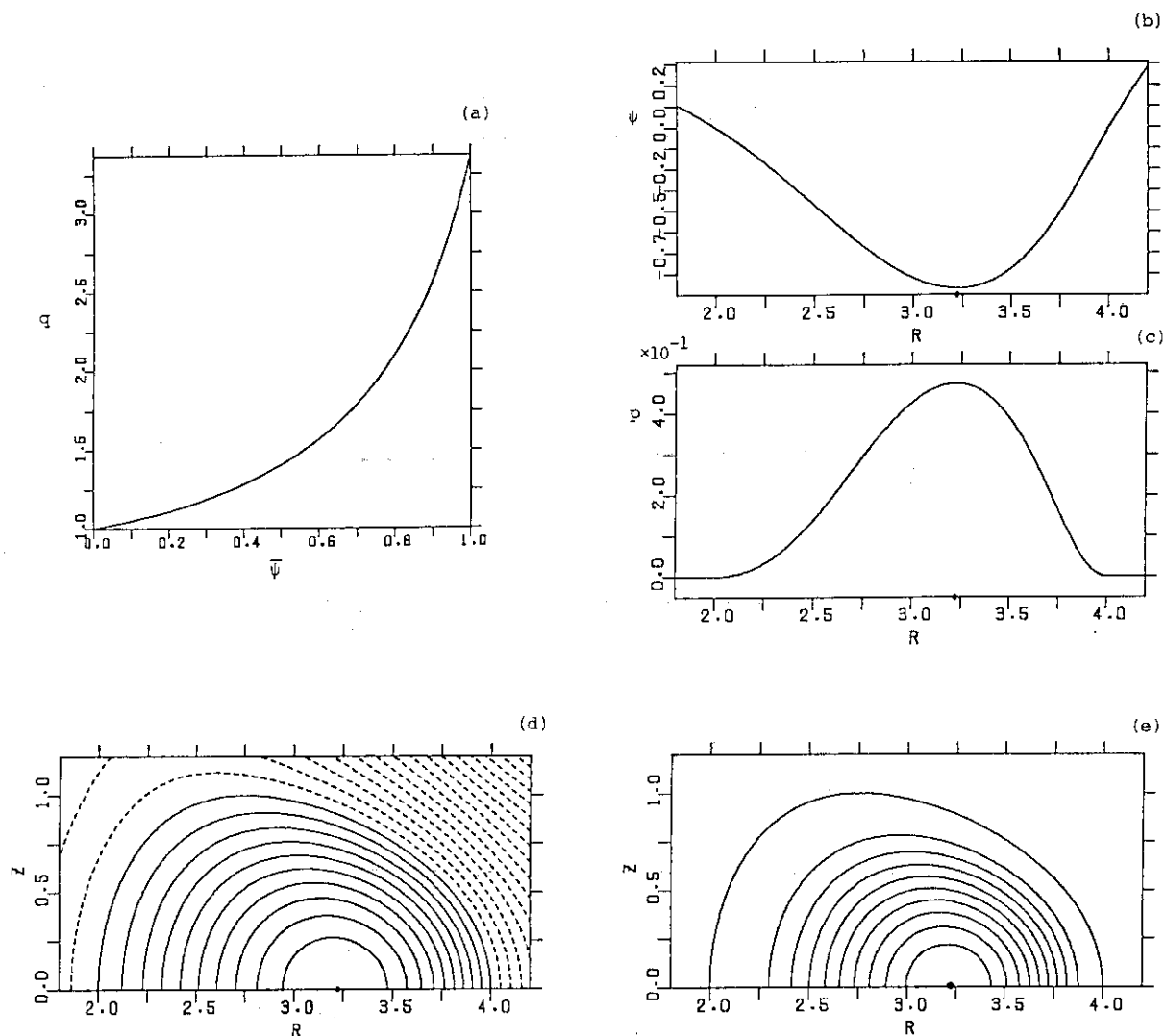


Fig.3 Static equilibrium with the surface defined by eq. (54) and  $R_0/a=3.0$ ,  $K=1$ , and  $\delta=0.25$ . The safety factor  $q=q(\bar{\psi})$ , the total pressure  $p=p(r,z=0)$  (Fig.5(b)) and the flux  $\psi=\psi(r,z=0)$  (Fig.5(c)) are displayed together with the contours of constant flux (Fig.5(d)) and pressure (Fig.5(e)), which coincide for this case.

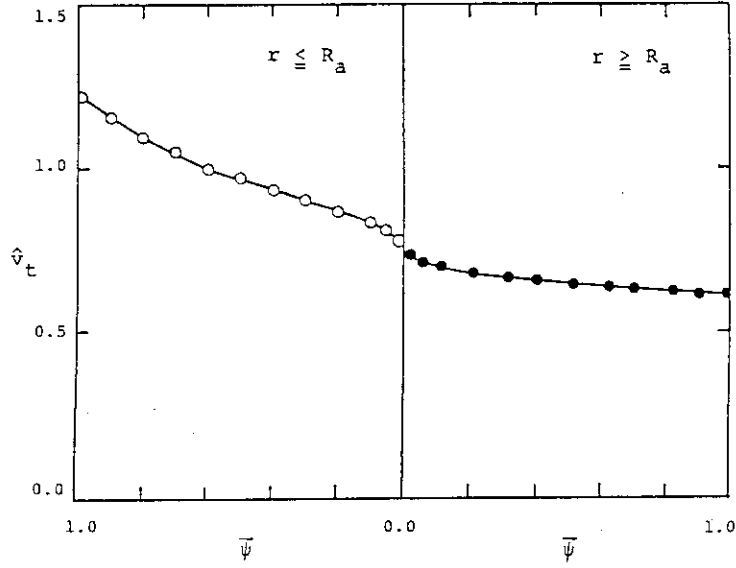


Fig.4 The toroidal flow derived from the total pressure with  $p_0(\bar{\psi})=0.5p(\bar{\psi})$  in the equilibrium shown in Fig.3. Two branches occur in reproducing  $p=p(r,z=0)$ .

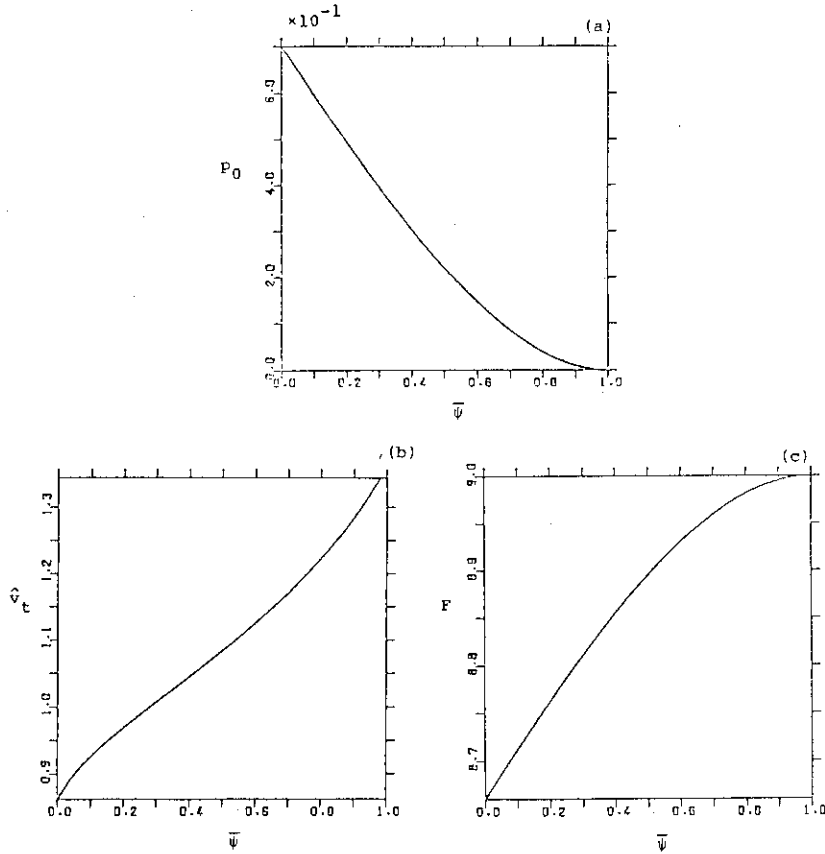


Fig.5 Equilibrium with toroidal flow. The pressure function  $p_0(\bar{\psi})$  has to be reduced by the factor 0.7 (Fig.5(a)) and the flow  $\hat{v}_t(\bar{\psi})$  by 2/3 (Fig.5(b)); the toroidal field  $F(\bar{\psi})$  is unchanged (Fig.5(c)). The safety factor  $q$  has a dip (Fig.5(d)). The total pressure  $p=p(r,z=0)$  (Fig.5(e)) and the poloidal flux  $\psi=\psi(r,z=0)$  (Fig.5(f)) are displayed as functions of  $r$  in the midplane  $z=0$ . The contour lines of constant flux and pressure do not coincide.

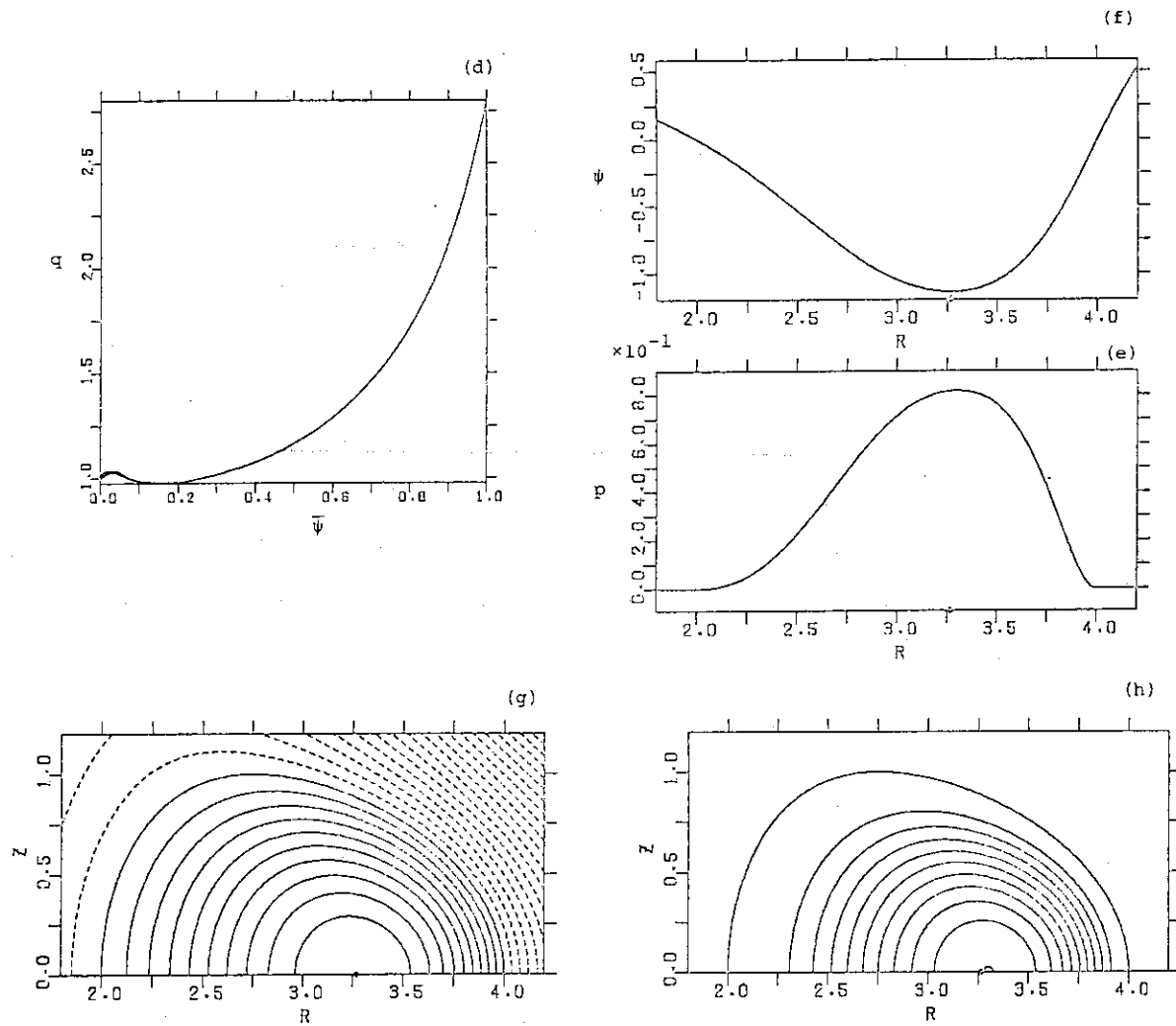


Fig. 5 (continue)

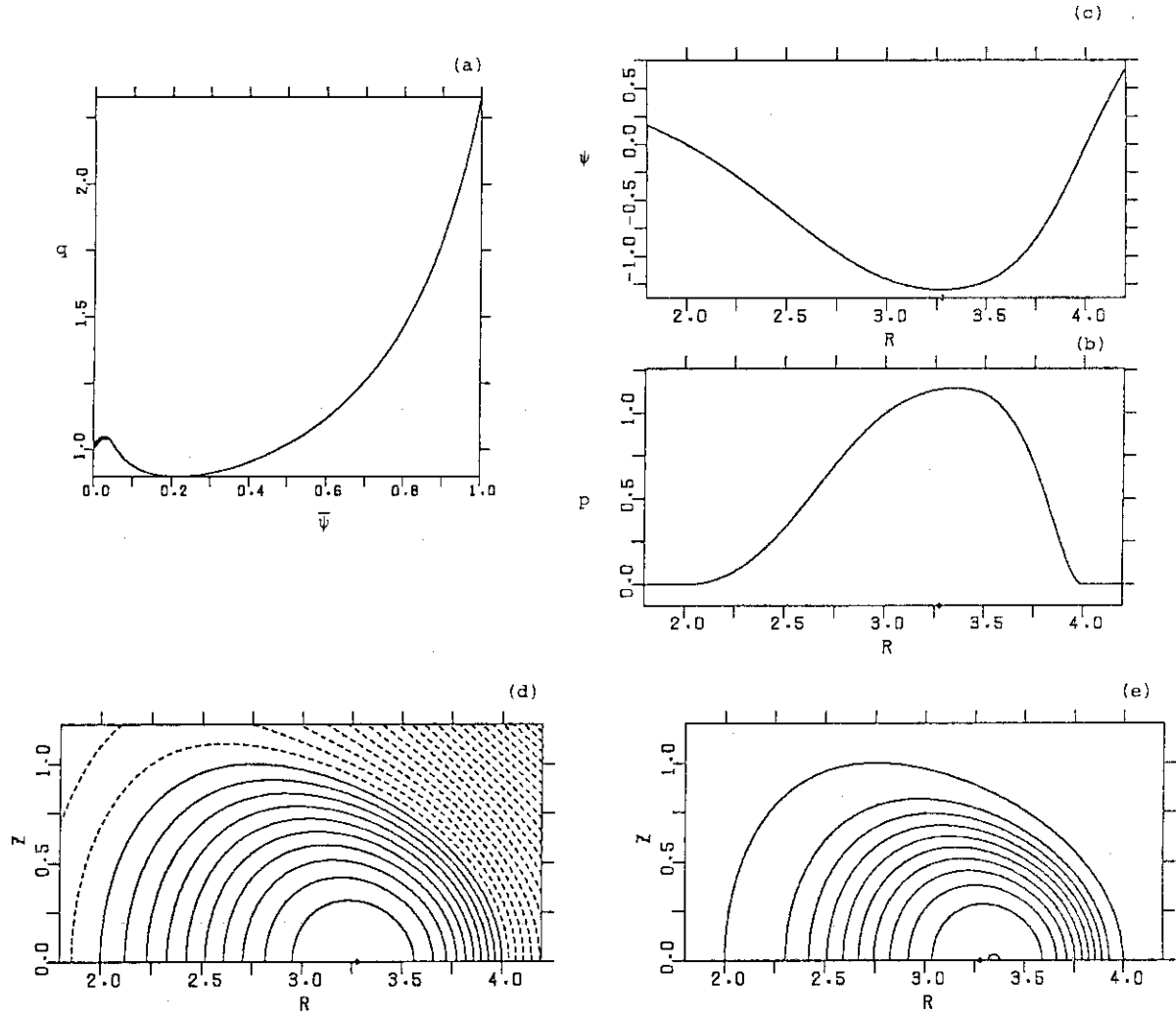


Fig.6 Equilibrium with toroidal flow. The pressure  $p_0$  flow and poloidal current profiles are the same as for Fig.5;  $p_0(\hat{v}_t)$  has to be multiplied by 0.65(0.75). The safety factor now has a pronounced dip (Fig.6(a)). The total pressure  $p=p(r,z=0)$  (Fig.6(b)) and the poloidal flux  $\psi=\psi(r,z=0)$  (Fig.6(c)) are displayed as functions of  $r$  in the midplane  $z=0$ . The contour lines of constant flux (Fig.6(d)) and pressure (Fig.6(e)) do not coincide.

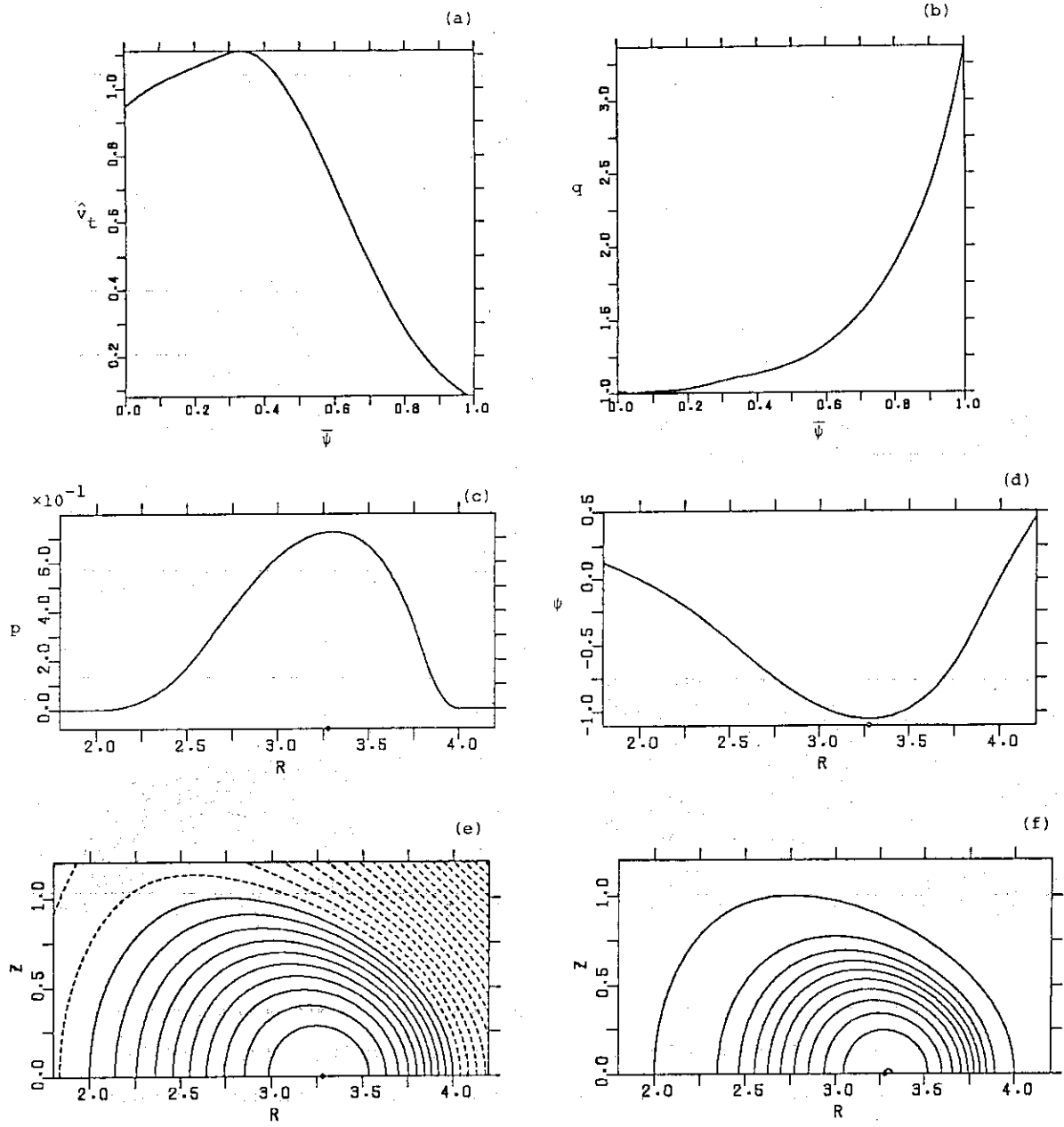


Fig.7 Equilibrium with toroidal flow. The  $p_0(\bar{\psi})$  and  $F(\bar{\psi})$  profiles are the same as for Fig.6; the flow has to be multiplied by the factor 0.5 (Fig.7(a)). The safety factor  $q$  is a smooth function (Fig.7(b)). The total pressure  $p=p(r,z=0)$  (Fig.7(c)) and the poloidal flux  $\psi=\psi(r,z=0)$  (Fig.7(d)) are displayed as functions of  $r$  in the midplane  $z=0$ . The contour lines of constant flux (Fig.7(e)) and pressure (Fig.7(f)) do not coincide.